



Achieving superior hydrogen storage properties of MgH_2 by the effect of TiFe and carbon nanotubes

Xiong Lu^a, Liuting Zhang^{a,*}, Haijie Yu^a, Zhiyu Lu^a, Jiahuan He^c, Jianguang Zheng^a, Fuying Wu^b, Lixin Chen^{c,*}

^a School of Energy and Power, Jiangsu University of Science and Technology, Zhenjiang 212003, China

^b Analysis and testing center, Jiangsu University of Science and Technology, Zhenjiang 212003, China

^c State Key Laboratory of Silicon Materials, Department of Materials Science and Engineering, Zhejiang University, Hangzhou 310027, China

ARTICLE INFO

Keywords:

Magnesium hydride
TiFe
Carbon nanotubes
Catalytic mechanism

ABSTRACT

Multiple catalysts have exhibited high activity on improving the hydrogen storage performance of magnesium hydride. Herein, TiFe as a superior catalyst was successfully prepared, and then doped into MgH_2 via ball milling to improve the de/rehydrogenation properties of MgH_2 at low temperatures. Compared with as-prepared MgH_2 , the onset desorption temperature could be reduced to 175 °C after adding 15 wt%-TiFe to MgH_2 . Furthermore, the 10 wt%-TiFe doped MgH_2 released approximately 6.5 wt% H_2 within 10 min at 300 °C, and 5.3 wt% H_2 could be rapidly absorbed at low temperature of 125 °C under hydrogen pressure of 3 MPa. Moreover, the additional doping of carbon nanotubes (CNTs) evenly distributed on the surface of MgH_2 particles, enabling the $\text{MgH}_2 + 10 \text{ wt\%-TiFe} + 5 \text{ wt\%-CNTs}$ composite with outstanding cycling performance. The activation energy of hydrogenation for MgH_2 was reduced from $72.5 \pm 2.7 \text{ kJ/mol}$ to $60.7 \pm 8.0 \text{ kJ/mol}$ after doping with TiFe and CNTs. However, the addition of TiFe and CNTs had limited influence on the thermodynamic properties of MgH_2 . The analysis of XRD, TEM, SEM and EDS indicated that uniformly distributed TiFe and CNTs served as active catalytic unit and aggregation preventer on enhancing the hydrogen storage properties of MgH_2 , respectively.

1. Introduction

Hydrogen energy is considered as one of the optimal candidates for achieving a carbon-neutral society due to its high energy density, non-toxic, environment-friendly and reproducibility. Nevertheless, a safe hydrogen storage technology with high density still restricts the development of a green hydrogen society. [1–3] Solid-state hydrogen storage is superior to gaseous hydrogen storage with high-pressure (35–70 MPa at room temperature) and liquid hydrogen storage at cryogenic temperature (–253 °C, 0.5–1 MPa) in terms of safety and density. [3–6]. Among various solid-state hydrogen storage materials, magnesium hydride (MgH_2) is widely investigated for its high volumetric (110 g/L) and gravimetric (7.6 wt%) contents, abundance of Mg element and cheap cost. [7,8]. Unfortunately, the slow hydrogen absorption and desorption rates and high desorption temperature (>300 °C) limit the practical application of MgH_2 . [9–12]. So far, to conquer above-mentioned problems, strategies such as surface modification, combination with other hydrides, nano-structuring and catalysts doping have

been attempted to tune the hydrogen absorption and desorption behaviors of MgH_2 at moderate conditions [13–21]. Among them, catalyst doping, which is considered as one of the most feasible modifying strategies, has significantly contributed to the promoted de/rehydrogenation kinetics of MgH_2 [22–28].

The hydrogen de/rehydrogenation kinetic parameter of MgH_2 was remarkably ameliorated by transition metal-based catalysts (TM: Ti, Ni, Co, Fe, etc.) [26,29–35]. Compared with other transition metals, Ti-related catalysts showed the highest catalytic effect on the behavior of de/rehydrogenation kinetics [36]. The identical results were further authenticated by Cui *et al.* [37] who studied the catalytic effect of various transition metal (Nb, V, Ti, Mo, and Ni) on modifying the hydrogen de/rehydrogenation activity of MgH_2 . In addition, Tian *et al.* [9] used liquid nitrogen frozen milling method to synthesize TiC nanoparticles (10 nm) and mixed them with MgH_2 . The thermogravimetry tests revealed that onset and peak dehydrogenation temperatures of the $\text{MgH}_2 + \text{TiC}$ (ball-milled 60 h) samples could be reduced to 190 and 275 °C, 228 and 159 °C lower than that of as-received MgH_2 , respectively. Nevertheless,

* Corresponding authors.

E-mail addresses: zhanglt89@just.edu.cn (L. Zhang), lxchen@zju.edu.cn (L. Chen).

<https://doi.org/10.1016/j.cej.2021.130101>

Received 29 January 2021; Received in revised form 19 April 2021; Accepted 23 April 2021

Available online 29 April 2021

1385-8947/© 2021 Published by Elsevier B.V.

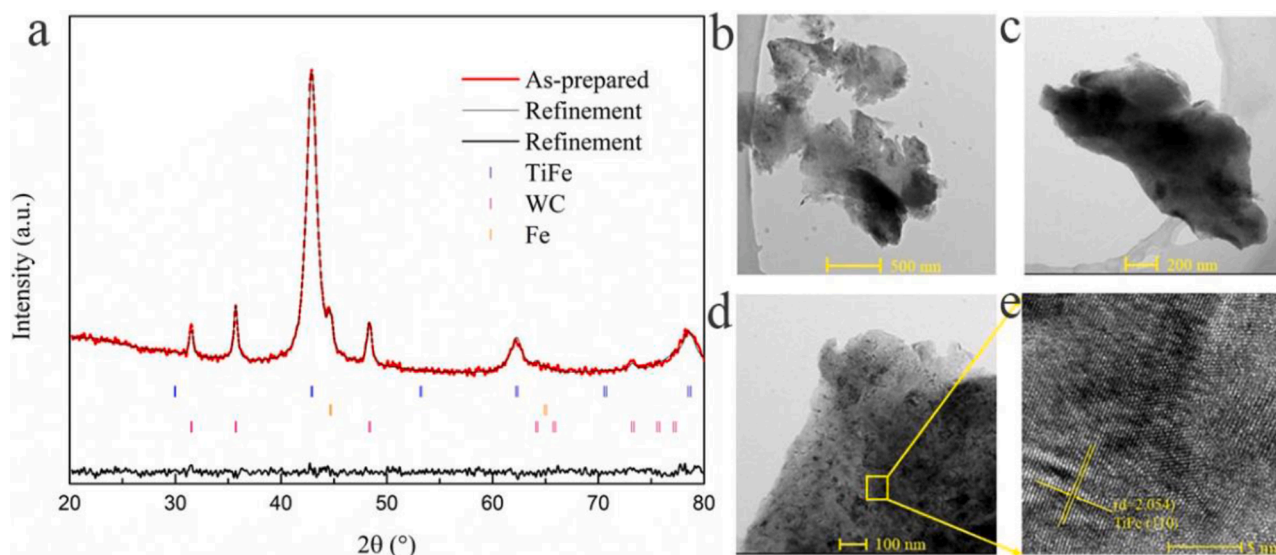


Fig. 1. XRD pattern (a), TEM images (b-d) and corresponding HRTEM image (e) of as-prepared TiFe.

Temitope and Shimizu et al. concluded that the addition of catalysts did not significantly tune the thermodynamic properties of MgH_2 . [38,39]

Recently, usage of Ti-based alloys to enhance hydrogen storage in MgH_2 catches considerable attention. Zhou et al. [40] reported that the hydrogen storage properties of MgH_2 could be enhanced by adding various Ti-based intermetallic alloys (TiAl, TiNi, Ti_3Al , TiFe, TiMn_2 , TiNb, and TiVMn). Further investigation found that TiMn_2 revealed the optimal catalytic activity while TiFe presented only moderate catalytic effect for de/rehydrogenation kinetics. Silva et al. prepared a Mg-TiFe nanocomposite by high-energy ball milling and thermal activation and evidenced that the composite started to absorb hydrogen at room temperature and finally took up 3.94 wt% H_2 within 15 h. [41] Though TiFe was demonstrated to greatly enhance the hydrogen de/absorption properties of MgH_2 , the large doping amount of TiFe decreased the practical hydrogen content of the composite to a value a bit lower than the requirement of DOE (5.0 wt%) [42,43]. Meanwhile, the practical application of Mg- MgH_2 system also faces the challenge of maintaining stable cycling performance. Previously, we found that transition metal modified MgH_2 system exhibited obvious declining cycle performance. [11] However, Gao et al. [44] revealed that the addition of CNTs could almost maintain the hydrogen absorption/desorption rate of MgH_2/FeB composites during cycling. Other reports also demonstrated that CNTs could remarkably improve the cycling performance of MgH_2/Ti bimetallic alloy. [45,46]

For the past two years, our group has proved the effect of an interesting strategy involves the use of nanoscale intermetallic transition metal alloys to further enhance the hydrogen storage properties of MgH_2 . By reducing the particle size of alloys to nanometer, we observed superior hydrogen storage properties of nano ZrMn_2 and $\text{LaNi}_{4.5}\text{Mn}_{0.5}$ catalyzed MgH_2 system. [47,48]. Thus, nanosized TiFe may significantly enhance the hydrogen storage functions of MgH_2 . Hence, TiFe nanoparticles were synthesized and the catalytic effect on MgH_2 was studied in this paper. For maintaining the cycling properties of TiFe modified MgH_2 system, carbon nanotubes were also adopted. Based on the microstructure evidence and hydrogen storage properties evaluation, a specific catalytic mechanism was proposed.

2. Experimental

2.1. Sample preparation

The original materials including Mg, Fe, Ti (99.99%, Sinopharm Chemical Reagent Co, Shanghai, China), and carbon nanotubes (CNTs

for short, Sigma-Aldrich, single-walled, 1.2–1.5 nm diameter, Carboxyl AP-grade) are commercially available.

The MgH_2 samples were prepared by hydrogenation heat treatment and mechanical ball milling. In brief, the Mg powders were hydrogenated by a Sieverts-type volumetric apparatus under 380 °C with a hydrogen pressure of 65 bar. Then, the samples were ball-milled at a speed of 450 rpm for 5 h with a ball-to-powder ratio (by weight) of 40:1 in a planetary ball mill system (QM-3SP4, Nanjing Chishun). Repeating the above steps twice and MgH_2 could be finally obtained. The particle size of as-prepared MgH_2 was approximately 1 μm observed from SEM image (Fig. S1).

The TiFe were prepared via a three steps method including sintering, mechanical ball milling and wet chemical ball milling according to previous reports [49]. In brief, 1.85 g Ti and 2.15 g Fe were heated to 500 °C under 2 MPa hydrogen pressure and then ball-milled in a wolfram carbide (WC) jar for 10 h. After the mixture was vacuum at 600 °C, oleic acid, heptane, and oleamide at a volume ratio of 1: 0.33: 20: 10 were added to the mixture and milled for another 60 h. The ball-to-material gravimetric proportion was 60:1 and rotation rate were 400 rpm. Water-free ethanol was used to wash slurry for 5 times in a high-rate centrifuge (8000 rpm, 6 min) to remove solvents. Finally, TiFe powders were gained through drying under vacuum for 10 h.

TiFe and MgH_2 were ball milled at 400 rpm with the ball-to-material gravimetric proportion of 40:1 for 4 h to get the $\text{MgH}_2 + \text{TiFe}$ composites. The composites were labeled as $\text{MgH}_2 + x \text{ wt\%TiFe}$, where x stood for the different amounts of TiFe ($x = 5, 10$, and 15). The $\text{MgH}_2 + 10 \text{ wt\%CNTs}$ sample was obtained by mixing the MgH_2 and CNTs at 400 rpm for 4 h. The $\text{MgH}_2 + 10 \text{ wt\%TiFe} + 5 \text{ wt\%CNTs}$ was prepared by ball milling CNTs with $\text{MgH}_2 + 10 \text{ wt\%TiFe}$ for 4 h.

2.2. Sample characterization

An X' Pert Pro X-ray diffractometer with Cu K α radiation ($\lambda = 1.5406 \text{ \AA}$, 40 kV, 40 mA) was applied to identify the phase compositions and structure of the samples from 20° to 80° with a scanning speed of 5°/min. In addition, the morphology and nanostructure of the samples were acquired using transmission electron microscope (TEM, Tecnai G2 F30 S-TWIN) and scanning electron microscope (SEM, Hitachi SU-70) measurements. Differential Scanning Calorimeter (DSC, Shimadzu Thermal Analysis System/TA-60WS-Japan) was used to conduct the thermal decomposition process of the samples at different heating rates (5, 8, 10, 12 °C/min) from 25 °C to 500 °C. Temperature Programed Dehydrogenation (TPD) was adopted to investigate the dehydrogenation

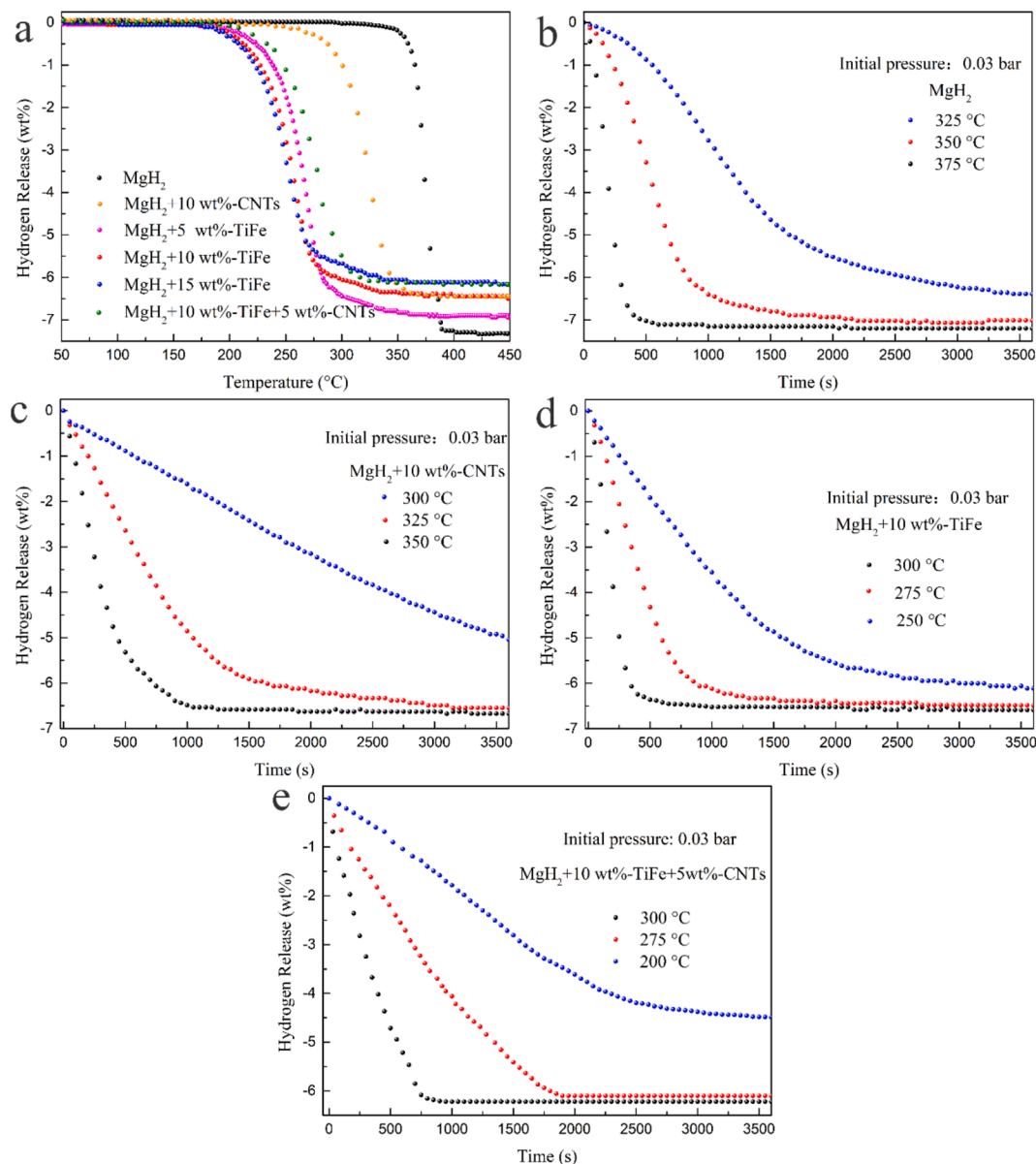


Fig. 2. Non-isothermal desorption curves (a) of MgH_2/TiFe , MgH_2/CNTs and $\text{MgH}_2/\text{TiFe}/\text{CNTs}$ composites, isothermal desorption curves of MgH_2 (b), $\text{MgH}_2 + 10$ wt%-CNTs (c), $\text{MgH}_2 + 10$ wt%-TiFe (d) and $\text{MgH}_2 + 10$ wt%-TiFe + 5 wt%-CNTs (e) at different temperatures.

behavior of samples at software-controlled temperatures.

The de/absorption hydrogen kinetics of the composites was studied using a self-made Sievert-type equipment. Approximately 160 mg of sample was loaded in a reactor with temperature and pressure sensors. For non-isothermal mode, the dehydrogenation experiments were implemented from 25 °C to 450 °C at a heating speed of 2 °C/min, and the hydrogenation examinations were carried from 25 °C to 400 °C at a heating rate of 1 °C/min under 3 MPa H_2 pressure. The pressure-composites-temperature (PCT) tests were conducted at different temperatures to seek equilibrium pressure. For isothermal ab/desorption tests, the samples were rapidly heated to a designed temperature and maintained constant. To prevent oxidation of the samples, all operation and transfers were handled in a MIKROUNA glove box filled with Ar, where the $\text{H}_2\text{O}/\text{O}_2$ content were maintained less than 0.1 ppm.

3. Results and discussion.

3.1. Characterization of as-prepared TiFe particles

Herein, TiFe was presented as an excellent catalyst to enhance the hydrogen storage properties of MgH_2 . X-ray diffraction (XRD) pattern of the as-synthesized sample was provided by Fig. 1a. The diffraction peak matched well with the PDF#19–0636 card of TiFe. According to the XRD refinement result, the contents of TiFe, WC (originating from the milling jar), and Fe in the as-prepared TiFe were calculated to be 92.17, 5.27 and 2.56 %. In addition, based on Scherrer equation $L = (K \lambda) / (\beta \cos \theta)$, the average grain size of as-prepared TiFe was estimated to be around 12 nm. Thus, the morphologies of TiFe particles were further studied by TEM. Fig. 1(b-c) showed that the particle size of TiFe was around 500 nm. In addition, the corresponding high-resolution TEM (HRTEM) shown in Fig. 1(d-e) demonstrated that interplanar distance between lattice fringes was 2.054 Å, which agreed well with the lattice planes (110) of TiFe.

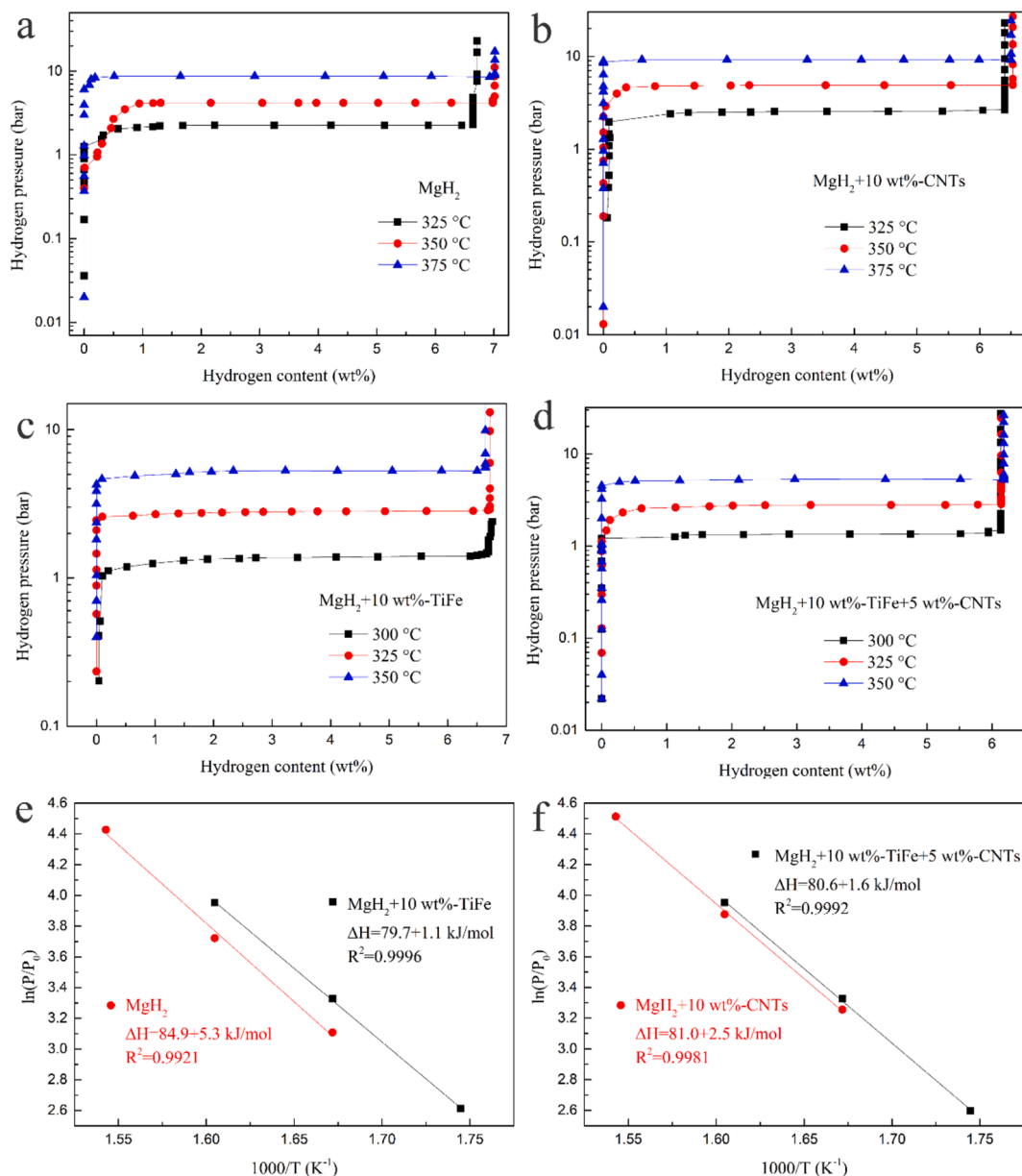


Fig. 3. The pressure-composites-temperature (PCT) curves of MgH_2 (a), $\text{MgH}_2 + 10 \text{ wt\%-CNTs}$ (b), $\text{MgH}_2 + 10 \text{ wt\%-TiFe}$ (c) and $\text{MgH}_2 + 10 \text{ wt\%-TiFe} + 5 \text{ wt\%-CNTs}$ (d) at different temperatures and corresponding van't Hoff plot (e) and (f).

3.2. Hydrogen storage performance of MgH_2/TiFe , MgH_2/CNTs and $\text{MgH}_2/\text{TiFe}/\text{CNTs}$ composites

$\text{MgH}_2/\text{CNTs}/\text{TiFe}$ samples were prepared by mechanical ball milling. To investigate the catalytic action of TiFe and CNTs on MgH_2 , Temperature Programmed Dehydrogenation (TPD) and DSC measurements were applied. For comparison, the dehydrogenation curves of as-prepared MgH_2 were also conducted, illustrated in Fig. 2. Fig. 2a presented the non-isothermal hydrogen desorption curves of $\text{MgH}_2/\text{TiFe}/\text{CNTs}$ composites. The as-prepared MgH_2 exhibited the highest onset and peak desorption temperature among all the samples, and its dehydrogenation process occurred between 305 °C ~ 385 °C. The addition of TiFe could remarkably reduce the initial temperature of desorption for MgH_2 . Specifically, the dehydrogenation process for $\text{MgH}_2 + 5 \text{ wt\%-TiFe}$ composite began at 200 °C. The initial temperature of hydrogen desorption for MgH_2 was further decreased with the increasing doping amount of TiFe. The addition of 10 wt%-TiFe and 15 wt%-TiFe respectively reduced the onset desorption temperature to 180 °C and 175 °C,

showing great catalyzing effect. Noteworthy, the more contents of TiFe were added, the lower dehydrogenation capacity was found. Besides, with the addition of 10 wt% CNTs, the onset decomposition temperature of MgH_2 decreased slightly to 260 °C. However, after co-doping CNTs and TiFe to MgH_2 , the $\text{MgH}_2 + 10 \text{ wt\%-TiFe} + 5 \text{ wt\%-CNTs}$ started to release hydrogen from 210 °C, around 30 °C higher than that of TiFe modified MgH_2 system.

Fig. 2(b-e) showed the isothermal dehydrogenation performance of as-prepared MgH_2 , $\text{MgH}_2 + 10 \text{ wt\%-CNTs}$, $\text{MgH}_2 + 10 \text{ wt\%-TiFe}$ and $\text{MgH}_2 + 10 \text{ wt\%-TiFe} + 5 \text{ wt\%-CNTs}$, respectively. For additive-free MgH_2 , 6.3 wt% hydrogen could be released at 325 °C within 60 min. Raising the temperature to 350 °C, the dehydrogenation speed of as-prepared MgH_2 became faster. At 375 °C, about 7.2 wt% hydrogen could be desorbed in 10 min. The $\text{MgH}_2 + 10 \text{ wt\%-CNTs}$ composite could desorb 4.9 wt% and 6.5 wt% H_2 at 300 °C and 325 °C in 1 h, respectively. At 350 °C, almost all the H_2 was released from the sample in 1100 s. Compared to the dehydriding kinetics of pure MgH_2 and $\text{MgH}_2 + 10 \text{ wt\%-CNTs}$, the $\text{MgH}_2 + 10 \text{ wt\%-TiFe}$ displayed enhanced

Table 1PCT parameters of the $\text{MgH}_2/\text{TiFe}/\text{CNTs}$ obtained at different temperatures.

Sample	Temperature (°C)	Desorption plateaus pressure (bar)	ΔH (kJ/mol)
MgH_2	325	2.27	84.9 +
	350	4.19	5.3
	375	8.70	
$\text{MgH}_2 + 10 \text{ wt\%-CNTs}$	325	2.63	81.0 +
	350	4.89	2.5
	375	9.24	
$\text{MgH}_2 + 10 \text{ wt\%-TiFe}$	300	1.38	79.7 +
	325	2.82	1.1
	350	5.28	
$\text{MgH}_2 + 10 \text{ wt\%-TiFe} + 5 \text{ wt\%-CNTs}$	300	1.36	80.6 +
	325	2.81	1.6
	350	5.32	

desorption kinetics and capacities. It was clearly seen from Fig. 2d that the $\text{MgH}_2 + 10 \text{ wt\%-TiFe}$ sample shows good hydriding kinetics with a hydrogen release capacity of 6.0 wt% within 1 h at the lowest testing temperature of 250 °C. In addition, TiFe modified MgH_2 released 6.6 wt% hydrogen in 10 min at 300 °C. The isothermal dehydrogenation curves of the $\text{MgH}_2 + 10 \text{ wt\%-TiFe} + 5 \text{ wt\%-CNTs}$ composite were also conducted, shown in Fig. 2e. In detail, it released 6.2 wt% H_2 within 14 min at 300 °C and 6.1 wt% H_2 in 30 min at 275 °C, respectively. Moreover, dehydrogenation was still possible at 250 °C, a capacity of 4.5 wt% was desorbed in 60 min for the $\text{MgH}_2 + 10 \text{ wt\%-TiFe} + 5 \text{ wt\%-CNTs}$ composite. Taking overall consideration between the desorption temperature and hydrogen content, the $\text{MgH}_2 + 10 \text{ wt\%-TiFe}$ started to desorb hydrogen at 180 °C and had a high dehydrogenation content of 6.6 wt%, showing the best dehydrogenation property.

The thermodynamic properties of TiFe and CNTs modified MgH_2 were further investigated by determining the equilibrium hydrogen pressures of MgH_2 , $\text{MgH}_2 + 10 \text{ wt\%-CNTs}$, $\text{MgH}_2 + 10 \text{ wt\%-TiFe}$ and

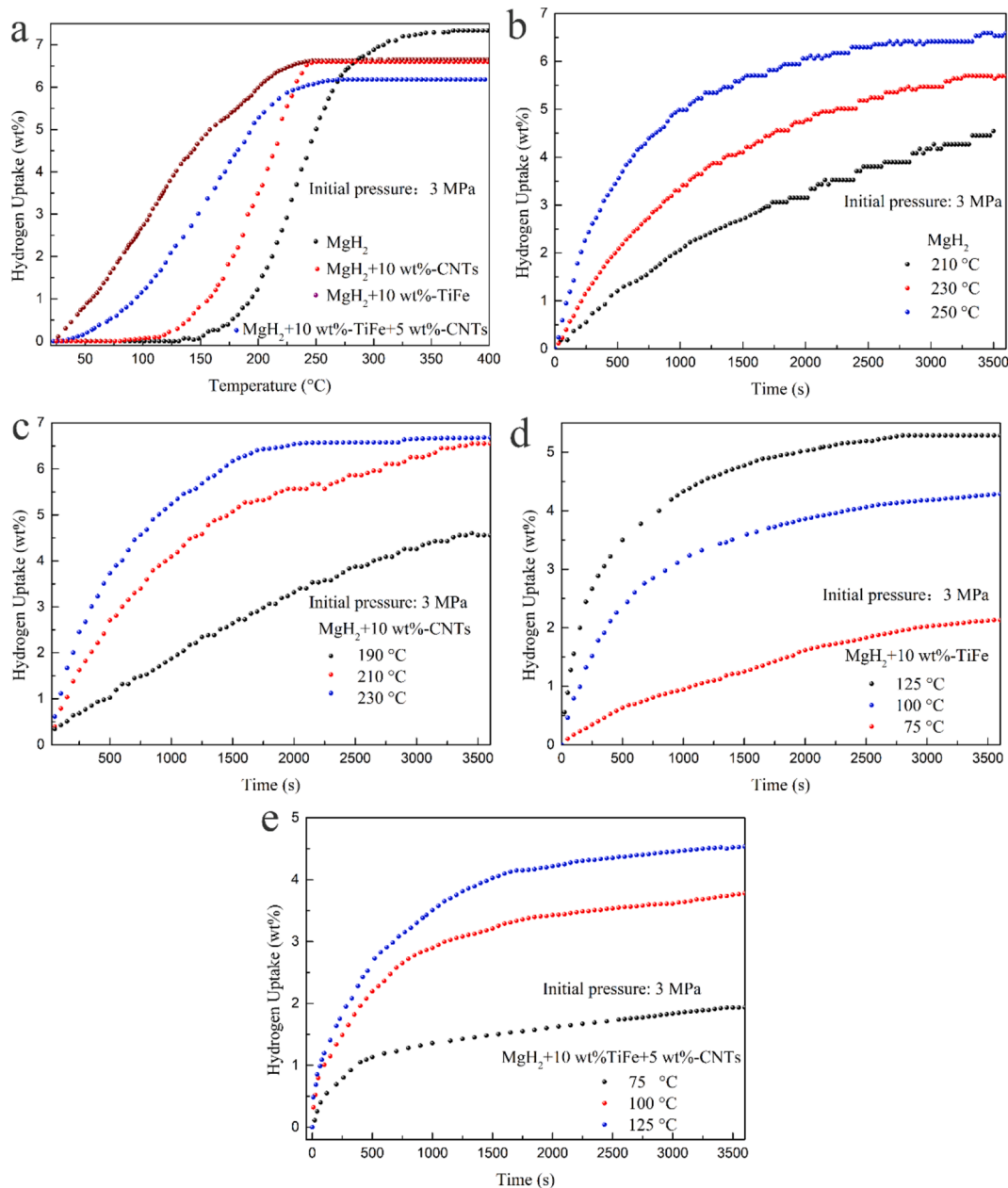


Fig. 4. Non-isothermal absorption curves (a) of MgH_2/TiFe , MgH_2/CNTs and $\text{MgH}_2/\text{TiFe}/\text{CNTs}$ composites, isothermal absorption curves of MgH_2 (b), $\text{MgH}_2 + 10 \text{ wt\%-CNTs}$ (c), $\text{MgH}_2 + 10 \text{ wt\%-TiFe}$ (d) and $\text{MgH}_2 + 10 \text{ wt\%-TiFe} + 5 \text{ wt\%-CNTs}$ (e) at different temperatures.

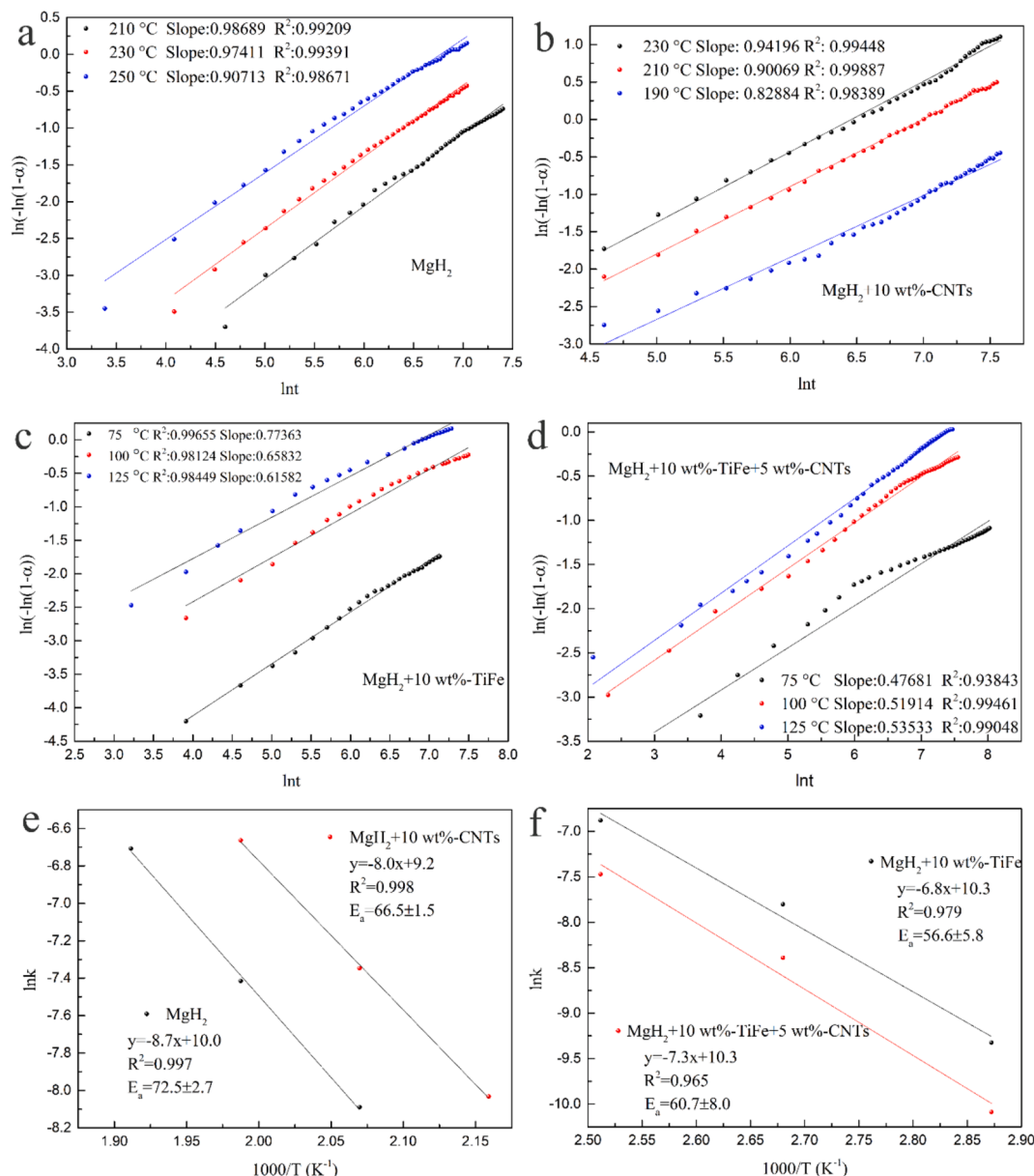


Fig. 5. isothermal hydrogenation JMAK curve plots of the prepared MgH₂ (a), MgH₂ + 10 wt%-CNTs (b), MgH₂ + 10 wt%-TiFe (c) and MgH₂ + 10 wt%-TiFe + 5 wt%-CNTs (d) at different temperatures samples, the fitted Arrhenius curve plots of MgH₂ and MgH₂ + 10 wt%-CNTs (e), MgH₂ + 10 wt%-TiFe and MgH₂ + 10 wt%-TiFe + 5 wt%-CNTs (f) samples.

MgH₂ + 10 wt%-TiFe + 5 wt%-CNTs at different temperatures, shown in Fig. 3(a-d). The desorption plateau pressures of MgH₂ were determined to be 2.27, 4.19 and 8.70 bar for 325 °C, 350 °C and 375 °C. As shown in Fig. 3b and 3c, the plateau pressures of MgH₂ + 10 wt%-TiFe were determined to be 1.38, 2.82 and 5.28 bar for 300 °C, 325 °C and 350 °C while those of MgH₂ + 10 wt%-CNTs were measured to be 2.63, 4.89 and 9.24 bar for 325 °C, 350 °C and 375 °C, respectively. In addition, the equilibrium pressure of MgH₂ + 10 wt%-TiFe + 5 wt%-CNTs at 300, 325, and 350 °C were observed to be 1.36, 2.81 and 5.32, respectively.

The detailed PCT data of MgH₂/TiFe/CNTs samples was summarized in table 1 and corresponding hydrogen decomposition enthalpy (ΔH) was calculated, presented in Fig. 3(e-f). The ΔH value of the MgH₂ was estimated to be 84.9 ± 5.3 kJ/mol. However, even with the addition of TiFe and CNTs, the calculated values of ΔH for MgH₂ + 10 wt%-CNTs (81.0 ± 2.5 kJ/mol), MgH₂ + 10 wt%-TiFe (79.7 ± 1.1 kJ/mol), and MgH₂ + 10 wt%-TiFe + 5 wt%-CNTs (80.6 ± 1.6 kJ/mol) were slightly lower than that of as-prepared MgH₂. Therefore, like other catalysts

reported before, [38,39] TiFe and CNTs could remarkably improve the kinetics performance but had little influence on the thermodynamic properties of MgH₂.

3.3. Catalytic action of TiFe, CNTs and TiFe + CNTs on hydrogen absorption of MgH₂

The influence of TiFe and CNTs on the hydrogen absorption of MgH₂ was examined under H₂ pressure of 3 MPa in iso/non-isothermal patterns. Fig. 4a displays the non-isothermal hydrogen absorption curves for the dehydrogenated MgH₂, MgH₂ + 10 wt%-CNTs, MgH₂ + 10 wt%-TiFe and MgH₂ + 10 wt%-TiFe + 5 wt%-CNTs samples. Under identical experimental conditions, the onset absorption hydrogen temperatures of these samples varied with each other. Concretely, the dehydrogenated pure-MgH₂ started to absorb H₂ at 150 °C. With the addition of CNTs and TiFe, the hydrogen absorption property of MgH₂ was improved. Notably, the hydrogenation in MgH₂ + 10 wt%-CNTs,

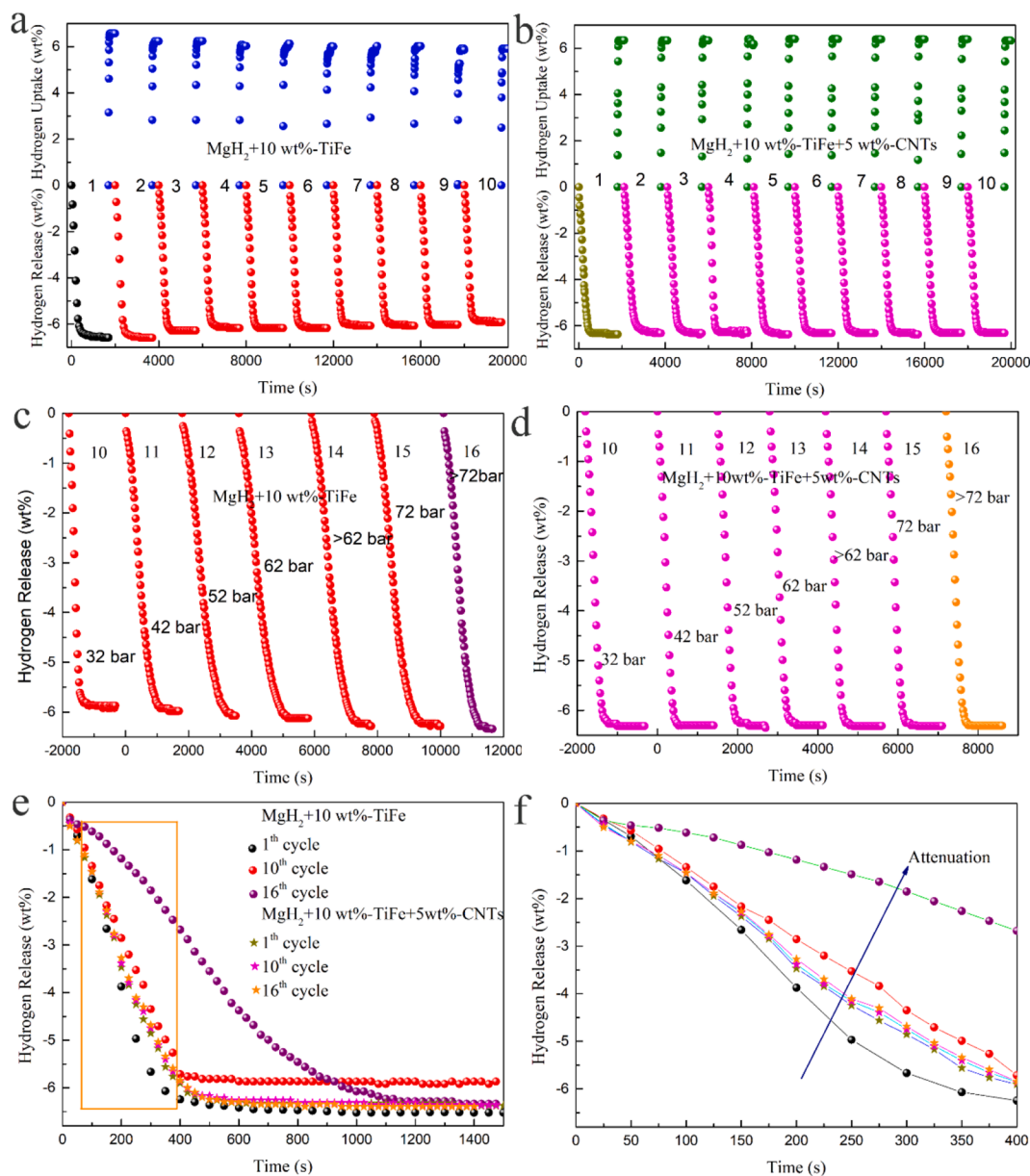


Fig. 6. Cycling profiles of $\text{MgH}_2 + 10 \text{ wt\%-TiFe}$ (a) and $\text{MgH}_2 + 10 \text{ wt\%-TiFe} + 5 \text{ wt\%-CNTs}$ (b) at 300°C (3 MPa for absorption), dehydrogenation profiles of $\text{MgH}_2 + 10 \text{ wt\%-TiFe}$ (c) and $\text{MgH}_2 + 10 \text{ wt\%-TiFe} + 5 \text{ wt\%-CNTs}$ (d) at 300°C (different hydrogen pressures for absorption), and different dehydrogenation profiles (e) and corresponding enlarged rectangle part (d) of $\text{MgH}_2 + 10 \text{ wt\%-TiFe}$ and $\text{MgH}_2 + 10 \text{ wt\%-TiFe} + 5 \text{ wt\%-CNTs}$.

$\text{MgH}_2 + 10 \text{ wt\%-TiFe}$, $\text{MgH}_2 + 10 \text{ wt\%-TiFe} + 5 \text{ wt\%-CNTs}$ occurred at 115°C , 25°C and 40°C , which was 35°C , 125°C , and 110°C lower than that of MgH_2 .

Isothermal hydrogenation tests shown in Fig. 4b presented that the dehydrogenated MgH_2 sample absorbed about 4.5 wt% H_2 in 1 h at 210°C . Even at high temperature of 250°C , 1 h was still needed to absorb 6.5 wt% hydrogen, showing relatively slow hydrogenation kinetics. For dehydrogenated $\text{MgH}_2 + 10 \text{ wt\%-CNTs}$ sample, approximately 4.5 wt%, 6.4 wt% and 6.4 wt% H_2 was charged within 60 min at 190°C , 210°C and 230°C under 3 MPa hydrogen pressure, respectively. Encouragingly, adding TiFe could dramatically enhance the hydrogenation kinetics of MgH_2 , as revealed by Fig. 4d. The $\text{MgH}_2 + 10 \text{ wt\%-TiFe}$ was able to take up 5.3 wt% hydrogen at 125°C within 60 min and 2 wt% H_2 could still be charged in 1 h at low temperature of 75°C . After co-doping TiFe and CNTs to MgH_2 , it was observed that the dehydrogenated $\text{MgH}_2 + 10 \text{ wt\%-TiFe} + 5 \text{ wt\%-CNTs}$ sample could take up 1.85 wt% and 3.6 wt% H_2 at 75°C and 100°C , respectively. When the

temperature raised to 125°C , the hydrogen absorption content was accumulated to 4.5 wt%. To further comprehend the enhancement of hydrogenation kinetics, E_a values of hydrogenation reaction was estimated according to the Arrhenius equation ($k = A \exp(E_a/RT)$). E_a interrelated with hydrogenation kinetics was quantitatively determined by the Johnson-Mehl-Avrami-Kolmogorov (JMAK) pattern: $\ln[-\ln(1-\alpha)] = \eta \ln(k) + \eta \ln(t)$, [43,44] where α represents the hydrogenation fraction of Mg spread into MgH_2 when the reaction time is t , k represents a transformation rate constant, and η is the growth of MgH_2 . In this case, the values of R^2 for isothermal hydrogenation curves were over 0.93 (Fig. 5(a-d)), indicating excellent linear relationship between the data. It should be noted in Fig. 5e that when 10 wt%-CNTs was introduced to MgH_2 , the value of E_a decreased from 72.5 ± 2.7 to 66.5 ± 1.5 kJ/mol. Upon further adding the catalyst, Fig. 5f shows that the value of E_a for the MgH_2 -10 wt%-TiFe composite was significantly reduced to 56.6 ± 5.8 kJ/mol, around 4.1 kJ/mol lower than that of $\text{MgH}_2 + 10 \text{ wt\%-TiFe} + 5 \text{ wt\%-CNTs}$ (60.7 ± 8.0 kJ/mol), implying that TiFe and CNTs could

Table 2
Different kinetic models for isothermal desorption.

Symbol	Model	Integral $f(\alpha)$ Form
D1	One-dimensional diffusion	α^2
D2	Two-dimensional diffusion	$\alpha + (1-\alpha)\ln(1-\alpha)$
D3	Three-dimensional diffusion (Jander equation)	$[1-(1-\alpha)^{1/3}]^2$
D4	Three-dimensional diffusion (Ginstling-Braunstein equation)	$(1-2\alpha/3)-(1-\alpha)^{2/3}$
F1	First-order reaction	$-\ln(1-\alpha)$
R2	Two-dimensional phase boundary	$1-(1-\alpha)^{1/2}$
R3	Three-dimensional phase boundary	$1-(1-\alpha)^{1/3}$
A2	Avrami-Erofe'ev	$[-\ln(1-\alpha)]^{1/2}$
A3	Avrami-Erofe'ev	$[-\ln(1-\alpha)]^{1/3}$

significantly decrease the activation energy and enhance the kinetics performance under identical hydrogenation situation.

3.4. Cycling properties of $\text{MgH}_2 + \text{CNTs}$, $\text{MgH}_2 + \text{TiFe}$, and $\text{MgH}_2 + \text{TiFe} + \text{CNTs}$

Except above superior hydrogen de/absorption properties of $\text{MgH}_2/\text{TiFe}/\text{CNTs}$ system, the cycling stability under moderate conditions was also highlighted. Cycling properties of $\text{MgH}_2 + 10 \text{ wt\%TiFe}$ composite were measured at 300°C (3 MPa hydrogen pressure for hydrogenation), exhibited in Fig. 6a. In detail, the composite released approximately 6.6 wt% hydrogen in 8 min, and rapidly absorbed hydrogen within 1 min at the first cycle. All cycles showed quick hydrogen sorption kinetics, however, the hydrogen storage content slowly reduced with the cycling number. In the 10th cycle, only about 5.8 wt% hydrogen capacity was maintained. Furthermore, increasing the operation hydrogen pressure resulted in increased hydrogen capacity (6.3 wt%), but the

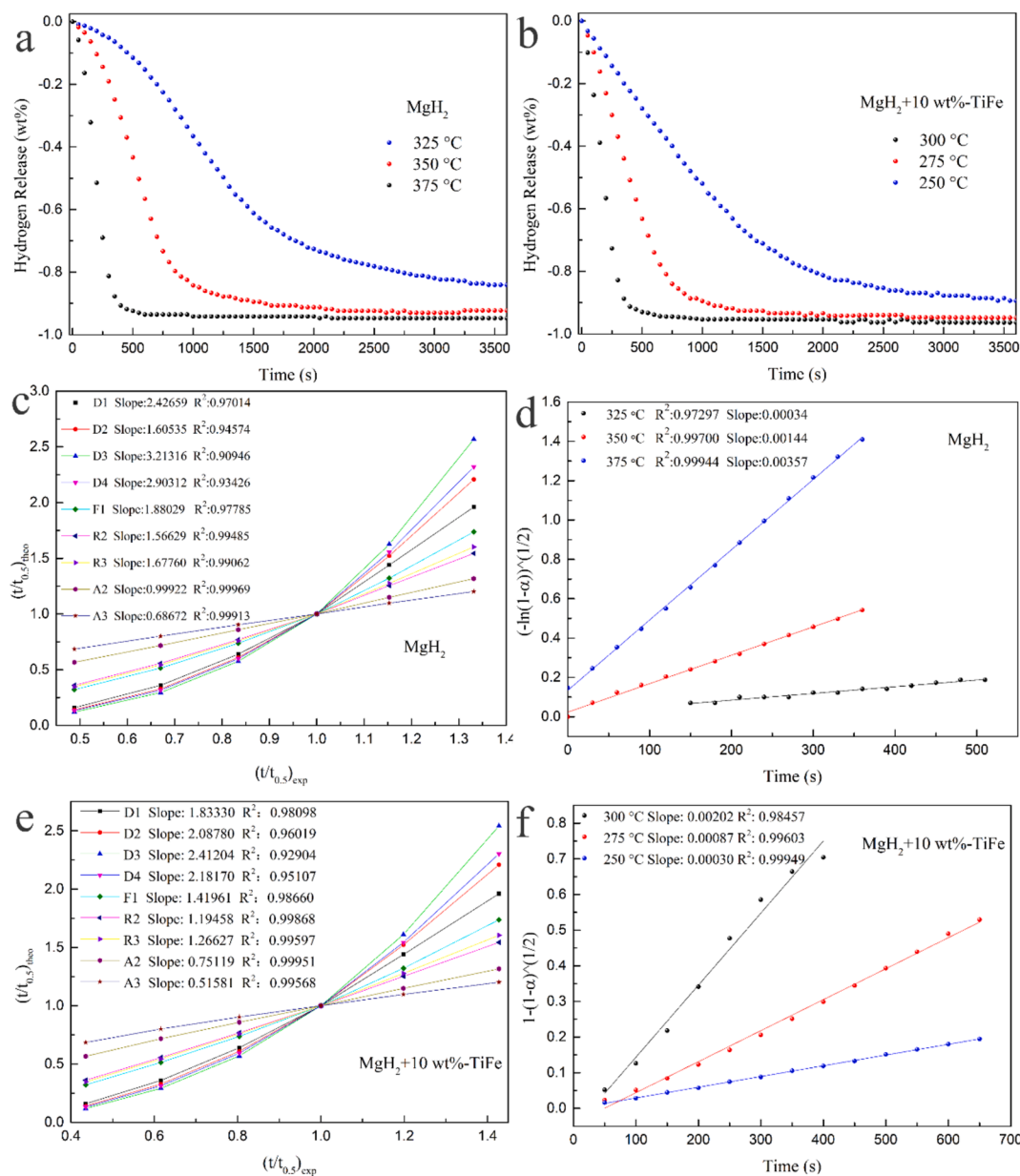


Fig. 7. Normalized isothermal dehydrogenation curves from prepared MgH_2 (a) and $\text{MgH}_2 + 10 \text{ wt\%TiFe}$ (b) at different temperatures, $(t/t_{0.5})_{\text{theo}}$ vs. $(t/t_{0.5})_{\text{exp}}$ diagram for MgH_2 at 375°C (c), the time dependence of the kinetic modeling equation for MgH_2 at different temperatures (d), $(t/t_{0.5})_{\text{theo}}$ vs. $(t/t_{0.5})_{\text{exp}}$ diagram for $\text{MgH}_2 + 10 \text{ wt\%TiFe}$ at 300°C (e), the time dependence of the kinetic modeling equation for $\text{MgH}_2 + 10 \text{ wt\%TiFe}$ at different temperatures (f).

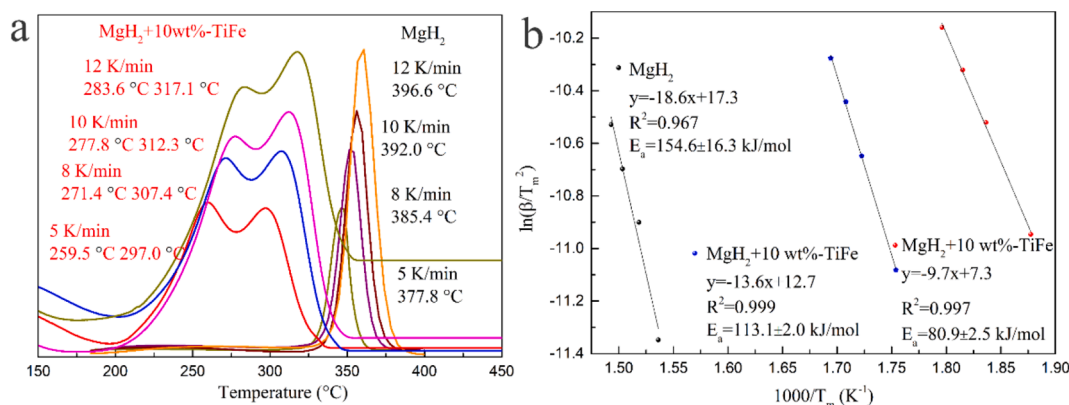


Fig. 8. DSC curves (a) of as-prepared MgH₂ and MgH₂ + 10 wt%-TiFe at various heating rates (5, 8, 10, and 12 °C/min) and estimations of the apparent active energies using the Kissinger method with the parameters obtained from DSC measurements (b).

dehydrogenation kinetics for the 16th cycle (with increased hydrogen pressure) was much slower (Fig. 6c and 6e), indicative of aggregation and/or growth in Mg/MgH₂ particles during cycling. With the addition of CNTs, the hydrogen storage capacity and kinetics of MgH₂ stayed stable without obviously decreasing after 10 cycles (Fig. S2). For the MgH₂ + 10 wt%-TiFe + 5 wt% CNTs composite, it was observed from Fig. 6b that the hydrogen capacity did not show any recession after 10th cycle. To simulate the practical charging condition, varying hydrogen pressures were adopted for the hydrogenation process (Fig. 6d). Though the hydrogen pressure was changed dramatically, the capacity and kinetics of last cycle were almost the same to that of the first cycle (6e and 6f), demonstrating that CNTs played a crucial role in preserving the good reversible property possessed by the MgH₂/TiFe composite.

3.5. Evolution of TiFe and CNTs during cycling and the catalytic mechanism

As mentioned above, TiFe showed remarkable catalytic action on the hydrogen storage performance of MgH₂. To uncover the mechanism behind dehydrogenation kinetics of the MgH₂ + 10 wt%-TiFe composite, experimental results were explained by different solid-state formula models, including growth, nucleation, geometric shrinkage, diffusion mobility, and reaction sequence. Sharp and Jones et al. [50,51] plotted the experimental data of (t/t_{0.5})_{exp} against the theoretical ones (t/t_{0.5})_{theo} to get a line and the value of fitted linear gradient for an optimal pattern should be close to 1. The kinetics process for isothermal hydrogen desorption of composite was identified by nine different dynamic models (Table 2) [52,53].

The normalized isothermal dehydrogenation plots were demonstrated in Fig. 7a and 7b. From these, the reaction extent α can be obtained during the process of dehydrogenation. The experimental data of (t/t_{0.5})_{exp} versus the theoretical values of (t/t_{0.5})_{theo} for MgH₂ and MgH₂ + 10 wt%-TiFe were plotted by different kinetic mechanisms, shown in Fig. 7c and 7e. For pure-MgH₂, the A2 model showed the best linear dependence with a slope of 0.9992. However, the addition of TiFe changed the kinetic equation from A2 to R2 (seen in Fig. 7e). This result implied that isothermal hydrogen desorption process of the MgH₂ + 10 wt%-TiFe followed a two-dimensional phase boundary pattern, dominated by geometric contraction and two-dimensional phase boundary diffusion. Moreover, the experimental curves at different temperatures matched well with the R2 model (R² > 0.98, Fig. 7f), further demonstrating that the dehydrogenation reaction at different temperatures could be commendably interpreted by the two-dimensional phase boundary model.

DSC measurements of MgH₂ + 10 wt%-TiFe composite and as-prepared MgH₂ were also investigated under various heating rates (5, 8, 10, 12 °C/min), revealed in Fig. 8a. It was obvious that the peak

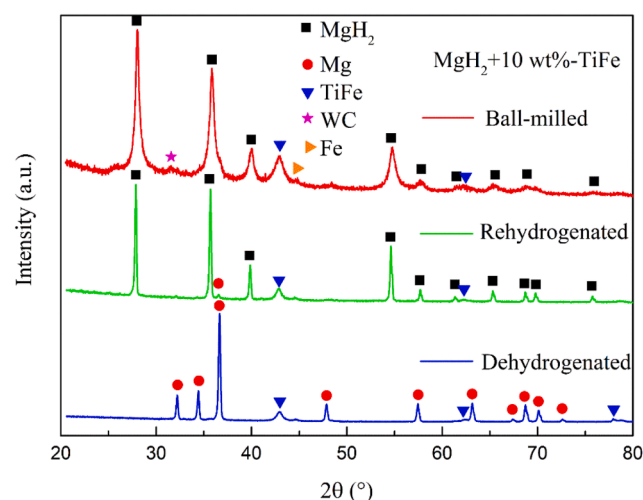


Fig. 9. XRD patterns of dehydrogenated and hydrogenated MgH₂ + 10 wt%-TiFe samples.

temperature of modified MgH₂ was substantially lower than that of pure MgH₂, testifying great catalytic influence of TiFe on improving the dehydrogenation property of MgH₂. In detail, the peak desorption temperature of MgH₂ + 10 wt%-TiFe was 259.5 (297.0) °C, 118.3 (80.8) °C lower than that of pure MgH₂ at heating speed of 5 °C/min. Two endothermic peaks occurred in the DSC curves, which might be caused by the inadequate contact between TiFe and MgH₂, just as reported in literature [54]. Moreover, the Kissinger formula was adopted to calculate the apparent activation energies (E_a) of hydrogen desorption for MgH₂ and MgH₂ + 10 wt%-TiFe composites [55]. The Kissinger's formula could be written as:

$$\ln(C/T_p^2) = -(E_a/(RT_p)) + A \quad (3-1)$$

Where C is the heating speed of the DSC measurement and T_p is the peak temperature. A is a temperature-independent constant, and R is the standard atmospheric constant. From the Kissinger plots in Fig. 8b, the values of E_a for the MgH₂ + 10 wt%-TiFe composite were computed to be 80.9 ± 2.5 and 113.2 ± 2.0 kJ/mol (for two steps each), much lower than 154.6 ± 16.3 kJ/mol of as-prepared MgH₂, which was competitive with other MgH₂-Ti/Fe based catalyst system [56-59]. The reduction in activation energy proved that the hydrogen decomposition energy barrier of MgH₂ could be reduced by TiFe nanoparticles, resulting in the superior hydrogen decomposition kinetics of MgH₂.

The actual catalytic efficiency of TiFe for MgH₂ usually concerns with the inherent activity and distribution position of the catalyst. In order to discover the evolution of TiFe in the hydrogen de/absorption

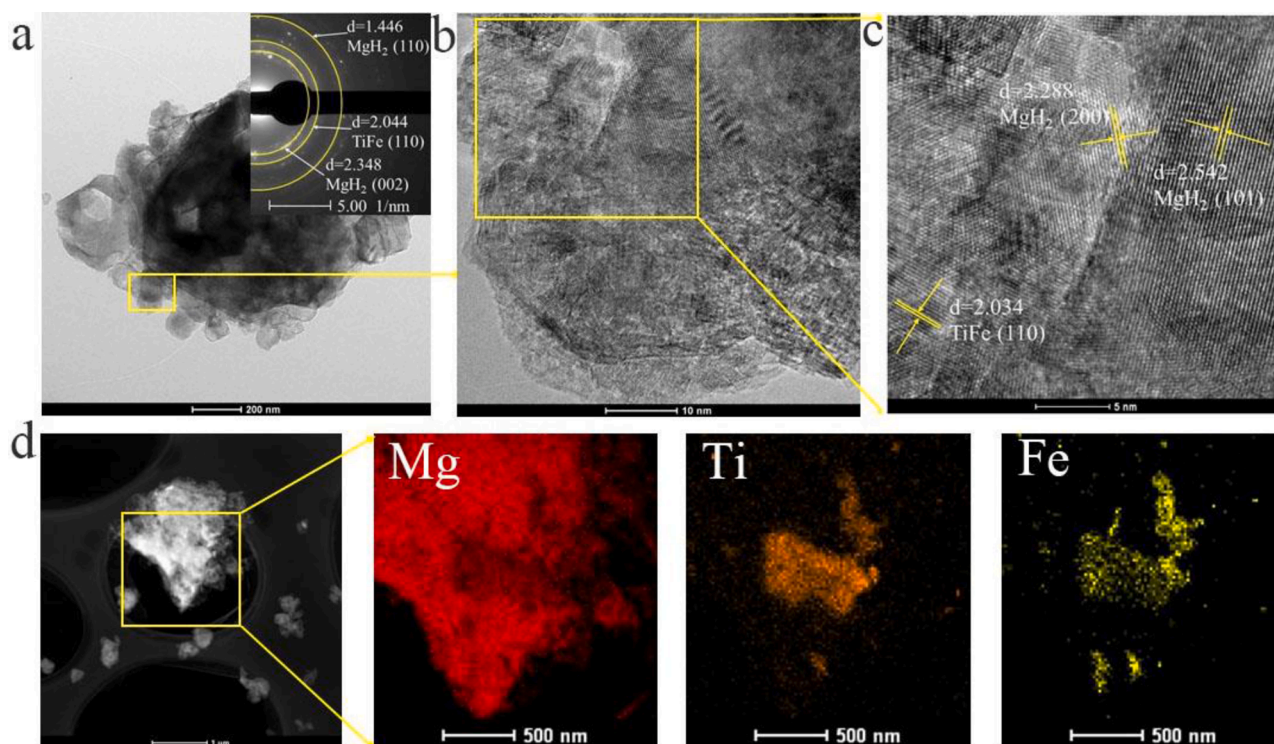


Fig. 10. TEM image with corresponding SAED pattern inset (a), HRTEM images (b-c), STEM-HAADF image and corresponding EDS mappings (d) of the MgH₂ + 10 wt%-TiFe composite.

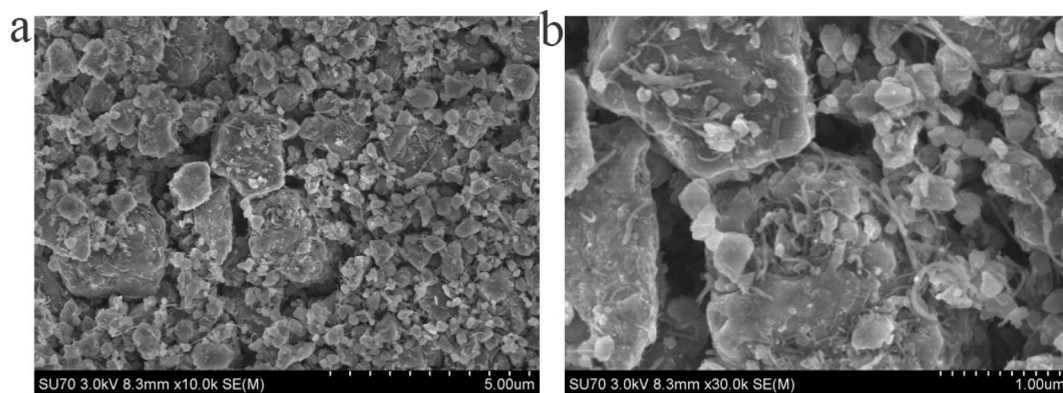


Fig. 11. SEM images of MgH₂ + 10 wt%-TiFe + 5 wt%-CNTs under different magnification.

process, XRD measurement was carried out. It can be observed from Fig. 9 and Fig. S3 that MgH₂ or Mg was the main phase after ball-milling, absorption or desorption, while TiFe phase remained stable. As the synthesized TiFe exhibited intermediate electronegativity between Mg and H (Ti (1.63), Fe (1.64), Mg (1.31), and H₂ (2.2)), it is very simple for TiFe ions to lose or obtain electrons (e⁻) than Mg ions or H⁺ ions, respectively, similar with previous report [60]. Hence, TiFe acted as an intermediate carrier for transferring electrons of Mg²⁺ and H⁺, promoting the hydrogen de/absorption process. Moreover, Fe was also occurred in the XRD patterns, which was responsible for the cycling degradation presented in Fig. 9a, agreed well with previous paper [11].

Furthermore, it could be observed from the TEM image in Fig. 10a that particle size of the MgH₂ + 10 wt%-TiFe was approaching 500 nm. According to corresponding SAED pattern, phases of TiFe (PDF#06-0696) and MgH₂ (PDF#12-0697) can be readily distinguished. The HRTEM patterns presented in Fig. 10(b-c) showed that the lattice spacing of 2.288 Å, 2.542 Å and 2.034 Å could be indexed as the (101), (200) planes of MgH₂ and (110) plane of TiFe, respectively.

Element of Ti and Fe were further identified by the energy-dispersive X-ray spectroscopy (EDS) mapping in Fig. 10d. TEM analyses indicated good distribution of TiFe nanoparticles in the MgH₂ matrix, serving as one of the important factors for the accelerated hydrogen diffusion along the Mg/MgH₂ interfaces. On the basis of above discussion, the striking enhancement of TiFe particles on the hydrogen storage performance of MgH₂ could be attributed to its intrinsic catalytic activity and well-distributed structure.

To shed light on the role of CNTs played in preserving the good hydrogen storage properties of the MgH₂ + 10 wt%-TiFe + 5 wt%-CNTs composite, SEM was adopted to characterize the distribution of CNTs in the composite. Fig. 11 revealed that CNTs were evenly distributed on the surface of MgH₂ + 10 wt%-TiFe. After cycling, it was obvious that the MgH₂ + 10 wt%-TiFe (Fig. S4) particles were agglomerated into massive particles, leading to the kinetic recession in cycling. With the help of CNTs, the tendency of Mg/MgH₂ particles to grow into large particles was effectively controlled, which contributed to preserve the good cycling properties of MgH₂.

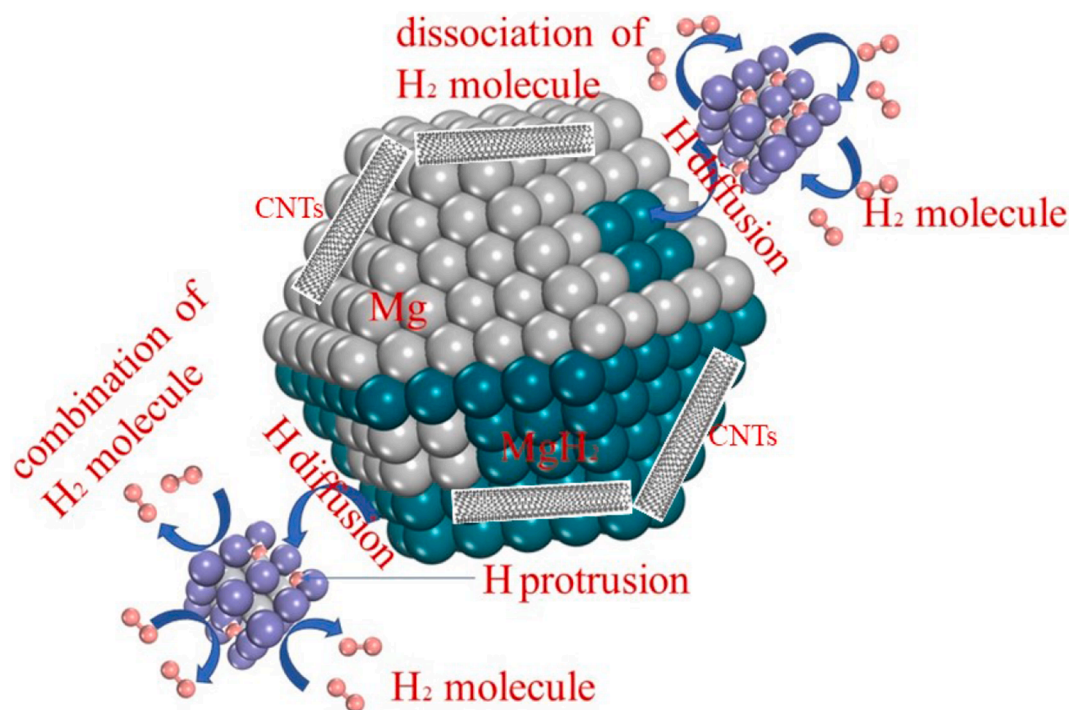


Fig. 12. Schematic summary of catalytic mechanism for the TiFe and CNTs catalyzed MgH_2 particles.

Combining the evidence from TPD, XRD, SEM, and TEM, the catalysis of TiFe and CNTs was illustrated in Fig. 12. The homogeneously distributed TiFe could be served as hydrogen pumps and effectively promoted the hydrogen diffusion along the Mg/MgH₂ interfaces, which could dramatically improve hydrogen storage performance of MgH₂. In detail, the hydrogen molecules were easily divided to hydrogen atoms at the surface of TiFe and combined with Mg particles to constitute MgH₂ in hydrogen absorption process. On the dehydrogenation process, the E_a value was reduced with the presence of TiFe, contributing to the decomposing of MgH₂ under low temperatures. In cycling, the evenly distributed CNTs prevented Mg/MgH₂ particles from aggregating, preserving stable cycle properties of the MgH₂ + 10 wt%-TiFe + 5 wt %-CNTs composite.

4. Conclusions

In this paper, TiFe particles was successfully prepared and an exciting catalytic activity on heightening the hydrogen storage performance of MgH₂ was evidenced. Experimental results demonstrated the MgH₂ + 10 wt%-TiFe began to desorb hydrogen at 180 °C and a hydrogen capacity of 6.6 wt% could be obtained within 10 min at 300 °C. The desorption activation energy of MgH₂ was reduced from 154.6 ± 16.3 to 80.9 ± 2.5 kJ/mol via the addition of TiFe. Importantly, the fully dehydrogenated MgH₂ + 10 wt%-TiFe was able to take up hydrogen from 25 °C, and exhibited pretty fast absorption kinetics. Additionally, the introduction of CNTs slowed the tendency of Mg/MgH₂ particles to aggregate, preserving stable cycle properties of MgH₂ + 10 wt%-TiFe system. The effect of TiFe and CNTs is responsible for the outstanding improvement on hydrogen storage performances of MgH₂, which may contribute to the design and development of high-performance hydrogen storage materials in near future.

Declaration of Competing Interest

The authors declare that they have no known competing financial interests or personal relationships that could have appeared to influence the work reported in this paper.

Acknowledgments

The authors would like to acknowledge financial support from the National Natural Science Foundation of China (Grant No. 51801078), the Natural Science Foundation of Jiangsu Province (Grant No. BK20180986).

Appendix A. Supplementary data

Supplementary data to this article can be found online at <https://doi.org/10.1016/j.cej.2021.130101>.

References

- [1] H. Shao, L. He, H. Lin, Progress and Trends in Mg-based Materials for Energy Storage Research: A Review, *Energy Technol.* 6 (2018) 445–448.
- [2] I.P. Jain, Hydrogen the fuel for 21st century, *Int. J. Hydrogen Energy* 34 (17) (2009) 7368–7378.
- [3] J. Zhang, S. Yan, H. Qu, Recent progress in magnesium hydride modified through catalysis and nanoconfinement, *Int. J. Hydrogen Energy* 43 (2018) 1545–1565.
- [4] X. Zhang, Y. Liu, X. Zhang, Empowering hydrogen storage performance of MgH₂ by nanoengineering and nanocatalysis, *Mater. Today Nano.* 9 (2020) 10064.
- [5] J. Zhang, S. Yan, H. Qu, Stress/strain effects on thermodynamic properties of magnesium hydride: A brief review, *Int. J. Hydrogen Energy* 42 (26) (2017) 16603–16610.
- [6] C.K. Kim, A review on design strategies for metal hydrides with enhanced reaction thermodynamics for hydrogen storage applications, *Int. J. Energy Res.* 42 (2018) 1455–1468.
- [7] T. Sadhasivam, H.-T. Kim, S. Jung, S.-H. Roh, J.-H. Park, H.-Y. Jung, Dimensional effects of nanostructured Mg/MgH₂ for hydrogen storage applications: A review, *Renew. Sustain. Energy Rev.* 72 (2017) 523–534.
- [8] M.S. El-Eskandarany, Recent developments in the fabrication, characterization and implementation of MgH₂-based solid-hydrogen materials in the Kuwait Institute for Scientific Research, *RSC Adv.* 9 (2019) 9907–9930.
- [9] M. Tian, C.X. Shang, Nano-structured MgH₂ catalyzed by TiC nanoparticles for hydrogen storage, *J. Chem. Technol. Biot.* 8 (2011) 69–74.
- [10] A. Bhatnagar, J.K. Johnson, M.A. Shaz, O.N. Srivastava, H₂ as a dynamic additive for improving the de/rehydrogenation properties of MgH₂: A combined experimental and theoretical mechanistic investigation, *J. Phys. Chem. C* 122 (2018) 21248–21261.
- [11] L. Zhang, L. Ji, Z. Yao, N. Yan, Z.e. Sun, X. Yang, X. Zhu, S. Hu, L. Chen, Facile synthesized Fe nanosheets as superior active catalyst for hydrogen storage in MgH₂, *Int. J. Hydrogen Energy* 44 (39) (2019) 21955–21964.
- [12] I.P. Jain, C. Lal, A. Jain, Hydrogen storage in Mg: A most promising material, *Int. J. Hydrogen Energy* 35 (10) (2010) 5133–5144.

- [13] S. Kumar, J. Ankur, J.S. Yamaguchi, Surface modification of MgH_2 by ZrCl_4 to tailor the reversible hydrogen storage performance, *Int. J. Hydrogen Energy* 42 (2017) 6152–6159.
- [14] S.A. Shevlin, Z.X. Guo, MgH_2 dehydrogenation thermodynamics: Nanostructuring and transition metal doping, *J. Phys. Chem. C* 117 (2013) 10883–10891.
- [15] L.Z. Ouyang, Z.J. Cao, H. Wang, Enhanced dehydrogenation thermodynamics and kinetics in $\text{Mg}(\text{In})$ - MgF_2 composite directly synthesized by plasma milling, *J. Alloy. Compd.* 586 (2014) 113–117.
- [16] H. Yong, S. Guo, Z. Yuan, Y. Qi, D. Zhao, Y. Zhang, Improved hydrogen storage kinetics and thermodynamics of RE-Mg-based alloy by co-doping Ce-Y, *Int. J. Hydrogen Energy* 44 (31) (2019) 16765–16776.
- [17] K. Alsabawi, E.M. Gray, C.J. Webb, The effect of ball-milling gas environment on the sorption kinetics of MgH_2 with/without additives for hydrogen storage, *Int. J. Hydrogen Energy* 44 (5) (2019) 2976–2980.
- [18] M. Zhang, X. Xiao, X. Wang, M. Chen, Y. Lu, M. Liu, L. Chen, Excellent catalysis of TiO_2 nanosheets with high-surface-energy {001} facets on the hydrogen storage properties of MgH_2 , *Nanoscale* 11 (2019) 7465–7473.
- [19] C. Zhou, R.C. Bowman Jr., Z.Z. Fang, J. Lu, L. Xu, P. Sun, H. Liu, H. Wu, Y. Liu, Amorphous TiCu-Based Additives for Improving Hydrogen Storage Properties of Magnesium Hydride, *ACS Appl. Mater. Interfaces* 11 (42) (2019) 38868–38879.
- [20] M. Ismail, M.S. Yahya, N.A. Sazelee, The effect of K_2SiF_6 on the MgH_2 hydrogen storage properties, *J. Magnes. Alloy.* 4 (2020) 832–840.
- [21] M. Ismail, Effect of LaCl_3 addition on the hydrogen storage properties of MgH_2 , *Energy* 79 (2015) 177–182.
- [22] Q.Q. Kong, H.H. Zhang, Z.L. Yuan, Hamamelis-like $\text{K}_2\text{Ti}_6\text{O}_{13}$ Synthesized by Alkali Treatment of Ti_3C_2 MXene: Catalysis for Hydrogen Storage in MgH_2 , *ACS Sustain. Chem. Eng.* 8 (2020) 4755–4763.
- [23] P.K. Soni, A. Bhatnagar, M.A. Shaz, O.N. Srivastava, Effect of graphene templated fluorides of Ce and La on the de/rehydrogenation behavior of MgH_2 , *Int. J. Hydrogen Energy* 42 (31) (2017) 20026–20035.
- [24] G. Chen, Y. Zhang, J. Chen, Enhancing hydrogen storage performances of MgH_2 by Ni nano-particles over mesoporous carbon CMK-3, *Nanotechnology* 29 (2018), 265705.
- [25] Y. Lu, H. Kim, K. Sakaki, S. Hayashi, K. Jimura, K. Asano, Destabilizing the Dehydrogenation Thermodynamics of Magnesium Hydride by Utilizing the Immiscibility of Mn with Mg, *Inorg. Chem.* 58 (21) (2019) 14600–14607.
- [26] Z. Ma, J. Zou, D. Khan, W. Zhu, C. Hu, X. Zeng, W. Ding, Preparation and hydrogen storage properties of MgH_2 -trimesic acid-TM MOF (TM=Co, Fe) composites, *J. Mater. Sci. Technol.* 35 (10) (2019) 2132–2143.
- [27] Y. Wang, Z. Ding, X. Li, S. Ren, S. Zhou, H. Zhang, S. Han, Improved hydrogen storage properties of MgH_2 by nickel@nitrogen-doped carbon spheres, *Dalton T.* 20 (2020) 3495–3502.
- [28] D. Peng, Z. Ding, Y. Fu, Enhanced H_2 sorption performance of magnesium hydride with hard-carbon-sphere-wrapped nickel, *RSC Adv.* 8 (2018) 28787–28796.
- [29] D. Pukazhselvan, K.S. Sandhya, D. Ramasamy, Transformation of Metallic Ti to TiH_2 Phase in the Ti/ MgH_2 Composite and Its Influence on the Hydrogen Storage Behavior of MgH_2 , *ChemPhysChem* 21 (2020) 1195–1210.
- [30] S.K. Verma, A. Bhatnagar, V. Shukla, Multiple improvements of hydrogen sorption and their mechanism for MgH_2 catalyzed through TiH_2 @Gr, *Int. J. Hydrogen Energy* 45 (2020) 19516–19530.
- [31] B.P. Tarasov, S.A. Mozkhukhin, A.A. Arbuzov, Features of the Hydrogenation of Magnesium with a Ni-Graphene Coating, *Russ. J. Phys. Chem.* 94 (2020) 996–1001.
- [32] R.R. Shahi, A.P. Tiwari, M.A. Shaz, O.N. Srivastava, Studies on de/rehydrogenation characteristics of nanocrystalline MgH_2 co-catalyzed with Ti, Fe and Ni, *Int. J. Hydrogen Energy* 38 (2013) 2778–2784.
- [33] K. Wang, Q. Deng, Constructing Core-Shell Co@N-Rich Carbon Additives Toward Enhanced Hydrogen Storage Performance of Magnesium Hydride, *Front. Chem.* 8 (2020) 233.
- [34] X. Ding, H. Ding, Y. Song, Activity-Tuning of Supported Co-Ni Nanocatalysts via Composition and Morphology for Hydrogen Storage in MgH_2 , *Front. Chem.* 7 (2020) 937.
- [35] L. Ji, L.T. Zhang, X.L. Yang, X.Q. Zhu, L.X. Chen, Remarkably improved hydrogen storage performance of MgH_2 by the synergistic effect of FeNi/rGO nanocomposite, *Dalton Trans.* 49 (2020) 4146–4154.
- [36] G. Liang, J. Huot, S. Boily, A. Van Neste, R. Schulz, Catalytic effect of transition metals on hydrogen sorption in nanocrystalline ball milled MgH_2 -Tm (Tm=Ti, V, Mn, Fe and Ni) systems, *J. Alloy. Compd.* 292 (1–2) (1999) 247–252.
- [37] J. Cui, J. Liu, H. Wang, Mg-TM (TM: Ti, Nb, V Co, Mo or Ni) core-shell like nanostructures: synthesis, hydrogen storage performance and catalytic mechanism, *J. Mater. Chem. A* 2 (2014) 9645–9655.
- [38] S.S. Temitope, A.J. Goudy, Dehydrogenation Kinetics and Modeling Studies of MgH_2 Enhanced by Transition Metal Oxide Catalysts Using Constant Pressure Thermodynamic Driving Forces, *Int. J. Hydrogen Energy* 37 (2012) 12301–12306.
- [39] Y. Shimizu, M. Otowaki, K. Shirai, Corrigendum to Consistency between the experimental formation entropy of MgH_2 and the spectroscopic entropy based on the third law of thermodynamics, *J. Alloy. Compd.* 30 (2019) 15206.
- [40] C.J. Zhou, Z.G.Z. Fang, Effect of Ti Intermetallic Catalysts on Hydrogen Storage Properties of Magnesium Hydride, *J. Phys. Chem. C* 25 (2013) 12973–12980.
- [41] R.A. Silva, R.L. Neto, D.R. Leiva, Room temperature hydrogen absorption by Mg and Mg-TiFe nanocomposites processed by high-energy ball milling, *Int. J. Hydrogen Energy* 43 (2018) 12251–12259.
- [42] R.A. Varin, Z. Zaranski, T. Czujko, The composites of magnesium hydride and iron-titanium intermetallic, *Int. J. Hydrogen Energy* 36 (2011) 1177–1183.
- [43] L. Klebanof, J. Keller, Final report for the DOE metal hydride center for excellence. 2012. SAND2012-0786.
- [44] S. Gao, X. Wang, H. Liu, et al., Effects of nano-composites (FeB, FeB/CNTs) on hydrogen storage properties of MgH_2 , *J. Power Sources* 438 (2019), 227006.
- [45] L.T. Zhang, Z. Sun, Z. Cai, Enhanced hydrogen storage properties of MgH_2 by the synergistic catalysis of $\text{Zr}_{0.4}\text{Ti}_{0.6}\text{Co}$ nanosheets and carbon nanotubes, *Appl. Surf. Sci.* 504 (2020), 144465.
- [46] K. Atikah, Y. Jia, Z.G. Chen, Effect of titanium based complex catalyst and carbon nanotubes on hydrogen storage performance of magnesium, *Sci. China-Chem* 004 (2013) 451–458.
- [47] L.T. Zhang, Z.L. Cai, Z.D. Yao, L. Ji, Z. Sun, N.H. Yan, B.Y. Zhang, B.B. Xiao, J. Du, X.Q. Zhu, L.X. Chen, A striking catalytic effect of facile synthesized ZrMn_2 nanoparticles on the de/rehydrogenation properties of MgH_2 , *J. Mater. Chem. A* 7 (2019) 5626–5634.
- [48] L.T. Zhang, X. Lu, Z. Sun, N.H. Yan, H.J. Yu, Z.Y. Lu, X.Q. Zhu, Superior catalytic effect of facile synthesized $\text{LaNi}_{4.5}\text{Mn}_{0.5}$ submicro-particles on the hydrogen storage properties of MgH_2 , *J. Alloy. Compd.* 844 (2020), 156069.
- [49] R.B. Falcao, E. Dammann, C. Rocha, Synthesis of TiFe Compound from Ball Milled TiH_2 and Fe Powders Mixtures, *Mater. Sci. Forum* 802 (2014) 61–65.
- [50] J.H. Sharp, G.W. Brindley, B.N.N. Achar, Numerical data for some commonly used solid state reaction equations, *J. Am. Ceram. Soc.* 49 (1966) 379–382.
- [51] L.F. Jones, D. Dollimore, T. Nicklin, Comparison of experimental kinetic decomposition data with master data using a linear plot method, *Thermochim Acta* 13 (1975) 240–245.
- [52] M. Liu, X. Xiao, S. Zhao, Facile synthesis of Co/Pd supported by few-walled carbon nanotubes as an efficient bidirectional catalyst for low temperature hydrogen storage properties of magnesium hydride, *J. Mater. Chem. A* 7 (2019) 5277–5287.
- [53] Q.G. Hang, H.W. Li, Y.T. Li, Intrinsic alterations in the hydrogen desorption of Mg_2NiH_4 by solid dissolution of titanium, *Dalton Trans.* 47 (2018) 8418–8426.
- [54] J. Liu, Z. Ma, Z. Liu, Synergistic effect of rGO supported Ni_3Fe on hydrogen storage performance of MgH_2 , *Int. J. Hydrogen Energy* 45 (2020) 16622–16633.
- [55] A.S. Gao, H. Wang, X.H. Wang, MoSe_2 hollow nanospheres decorated with FeNi_3 nanoparticles for enhancing the hydrogen storage properties of MgH_2 , *J. Alloy. Compd.* 830 (2020), 154631.
- [56] N.A. Ali, N. Hayatiidris, M.F. Mddin, Nanolayer-like-shaped MgFe_2O_4 synthesised via a simple hydrothermal method and its catalytic effect on the hydrogen storage properties of MgH_2 , *RSC Adv.* 8 (2018) 15667–15674.
- [57] N.A. Sazelee, N.H. Idris, M.F.M. Din, Synthesis of $\text{BaFe}_{12}\text{O}_{19}$ by solid state method and its effect on hydrogen storage properties of MgH_2 , *Int. J. Hydrogen Energy* 43 (2018) 20853–20860.
- [58] M. Ismail, N.S. Mustafa, N.A. Ali, The hydrogen storage properties and catalytic mechanism of the CuFe_2O_4 -doped MgH_2 composite system, *Int. J. Hydrogen Energy* 44 (2018) 318–324.
- [59] Z.Y. Wang, X.L. Zhang, Z.H. Ren, Y. Liu, In situ formed ultrafine NbTi nanocrystals from a NbTiC solid-solution MXene for hydrogen storage in MgH_2 , *J. Mater. Chem. A* 7 (2019) 14244.
- [60] L.T. Zhang, X.Z. Xiao, C.C. Xu, J.G. Zheng, X.L. Fan, J. Shao, S.Q. Li, H.W. Ge, Q. D. Wang, L.X. Chen, Remarkably Improved Hydrogen Storage Performance of MgH_2 Catalyzed by Multi-valence NbH_x Nanoparticles, *J. Phys. Chem. C* 119 (2015) 8554–8562.